#### **POLYMERS**

# Polymeric multimaterials by photochemical patterning of crystallinity

Adrian K. Rylski<sup>1</sup>, Henry L. Cater<sup>1</sup>†, Keldy S. Mason<sup>1</sup>†, Marshall J. Allen<sup>1,2</sup>†, Anthony J. Arrowood<sup>2</sup>, Benny D. Freeman<sup>2</sup>, Gabriel E. Sanoja<sup>2</sup>, Zachariah A. Page<sup>1</sup>\*

An organized combination of stiff and elastic domains within a single material can synergistically tailor bulk mechanical properties. However, synthetic methods to achieve such sophisticated architectures remain elusive. We report a rapid, facile, and environmentally benign method to pattern strong and stiff semicrystalline phases within soft and elastic matrices using stereocontrolled ring-opening metathesis polymerization of an industrial monomer, *cis*-cyclooctene. Dual polymerization catalysis dictates polyolefin backbone chemistry, which enables patterning of compositionally uniform materials with seamless stiff and elastic interfaces. Visible light–induced activation of a metathesis catalyst results in the formation of semicrystalline *trans* polyoctenamer rubber, outcompeting the formation of *cis* polyoctenamer rubber, which occurs at room temperature. This bottom-up approach provides a method for manufacturing polymeric materials with promising applications in soft optoelectronics and robotics.

ultimaterial structures that synergistically combine stiff and elastic components are ubiquitous in living systems, providing unparalleled combinations of mechanical properties (e.g., strength, toughness, and durability) (*1–3*). However, creating synthetic materials with integrated stiff and elastic domains remains an ongoing challenge (*4–6*). A scalable solution to achieving such structures would prove transformative for fundamental and applied research in soft materials and in advanced technologies that benefit from

compliant, tough, and lightweight objects, such as programmable actuators (7) and bioelectronics (8). State-of-the-art strategies to pattern stiffness rely on spatially varying the cross-link density of polymer networks using orthogonal two-stage and/or wavelengthselective lithographic curing processes (9–14). However, costly fabrication, material waste, brittle failure, and/or incumbent interfacial stress preclude access to synthetic materials and structures that mimic those found ubiquitously in nature. Herein, we overcome these limitations using a single, inexpensive feedstock to photopattern stiff and strong domains within a soft and elastic matrix using dual-initiated, stereo-controlled ring-opening metathesis polymerization (ROMP) of an olefinic monomer, *cis*-cyclooctene (COE) (Fig. 1A).

Twelve ruthenium (Ru)-based catalysts were screened and characterized in terms of reactivity and stereochemical control during ROMP (Fig. 1B and fig. S11). The use of COE as a low-viscosity liquid enabled bulk polymerizations (>99 vol % COE), minimizing hazardous solvent waste and postprocessing requirements. The trans: cis alkene ratios were characterized using <sup>1</sup>H nuclear magnetic resonance (NMR) spectroscopy, integrating the two peaks between ~5.3 and 5.4 parts per million (ppm), narrowing the catalyst scope to those that resulted in either high trans- or cis-alkene content (Fig. 1C, table S1, and fig. S12). Three representative catalysts were selected for further study: (i) Grubbs second generation (G2) as a control, (ii) a thermally latent bis-N-heterocyclic carbene (bis-NHC) catalyst (15) (Ru-1), and (iii) a stereoretentive catalyst (16) (Ru-2) (tables S1 to S3 and fig. S13). The use of G2 (50 ppm relative to COE, ~23°C, <5 min) resulted in complete COE consumption to produce trans polyoctenamer rubber

<sup>1</sup>Department of Chemistry, The University of Texas at Austin, Austin, TX 78712, USA. <sup>2</sup>McKetta Department of Chemical Engineering, The University of Texas at Austin, Austin, TX 78712. USA.

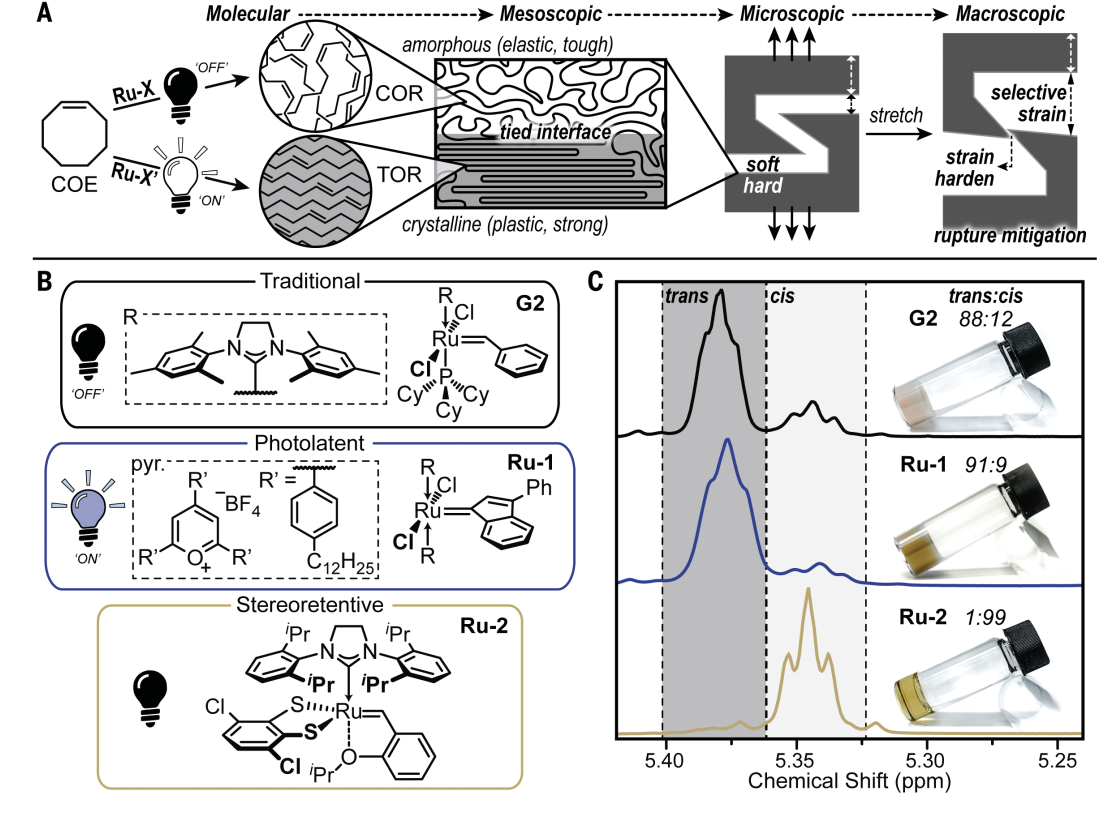
\*Corresponding author. Email: zpage@utexas.edu †These authors contributed equally to this work.

# Fig. 1. Control over polyoctenamer stereochemistry.

(A) Bottom-up design of synthetic materials with patterned crystal-linity from a single feedstock, COE, to provide TOR or COR.
(B) Chemical structures for Ru-alkylidene catalysts examined for ROMP of approximately neat COE. (C) <sup>1</sup>H NMR spectra for polyoctenamer produced using G2, Ru-1 + pyr. + light, and Ru-2 (<100 ppm catalyst) showing the signals corresponding to *trans* and *cis* isomers. Insets: *trans:cis* 

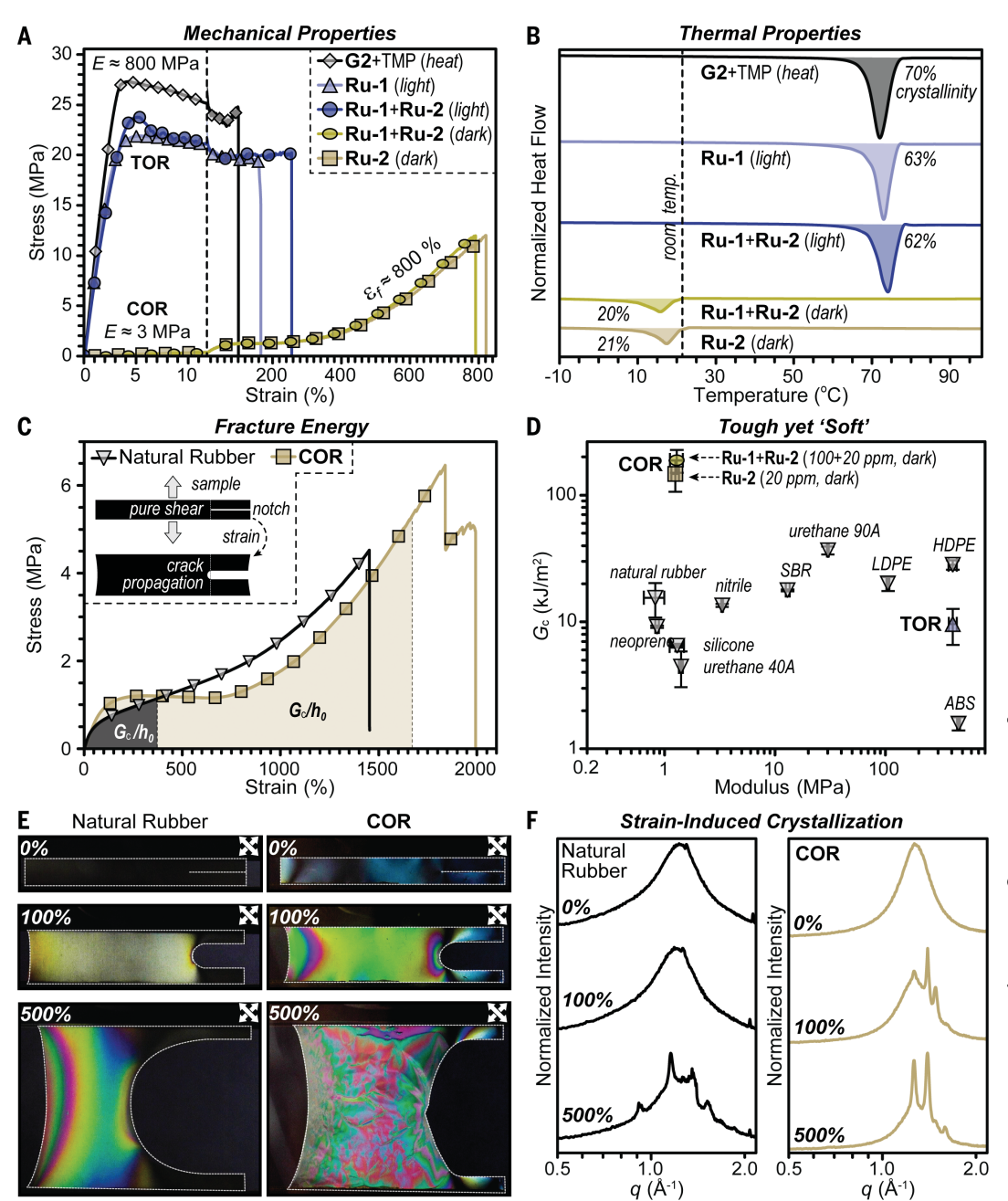
ratios and representative

images of polyoctenamer.



1 of 5

Fig. 2. Bulk thermomechanical analyses of polyoctenamer rubbers. (A) Stress-strain curves from uniaxial elongation until failure, with representative E and  $\epsilon_{\text{f}}$  values indicated. Scale was expanded for the low-deformation range, and symbols are indexed for clarity. (B) Differential scanning calorimetry to characterize melting temperature and percent crystallinity. Parenthetical terms "heat," "light," and "dark" indicate fabrication conditions. (C) Representative stress-strain curves for COR and natural rubber used to calculate  $G_c$ . as defined in the shaded regions. Symbols are indexed for clarity. (**D**) Comparison of COR and TOR with commercial rubbers and plastics as a function of  $G_c$  and modulus. Data points represent an average of at least three notched and three notch-free samples with error bars of ±1 SD from the mean. (E) Straininduced crystallization for natural rubber and COR as visualized through crossed polarizers and (F) measured using WAXS.



(TOR) with ~85% *trans*-alkene content, whereas Ru-1 (50 ppm relative to COE, ~100°C, 60 min) resulted in ~78% *trans*-alkene content. This result suggested that latent activation of Ru-1 could enable selective TOR synthesis.

To facilitate spatial control over the stereochemistry of polyoctenamer, Ru-1 was examined for photolatency (figs. S14 and S15). Inspired by the work of Rovis and co-workers (17) on the use of pyrylium photoredox catalysis for ROMP, a pyrylium derivative, 2,4,6-tris(4-dodecylphenyl) pyrylium tetrafluoroborate (hereafter pyr.) (Fig. 1B), was synthesized to provide solubility in COE (figs. S16 to S23) and used to activate bis-NHC catalysts bearing indenylidene (Ru-1), benzylidene, or alkenylcarbene groups with

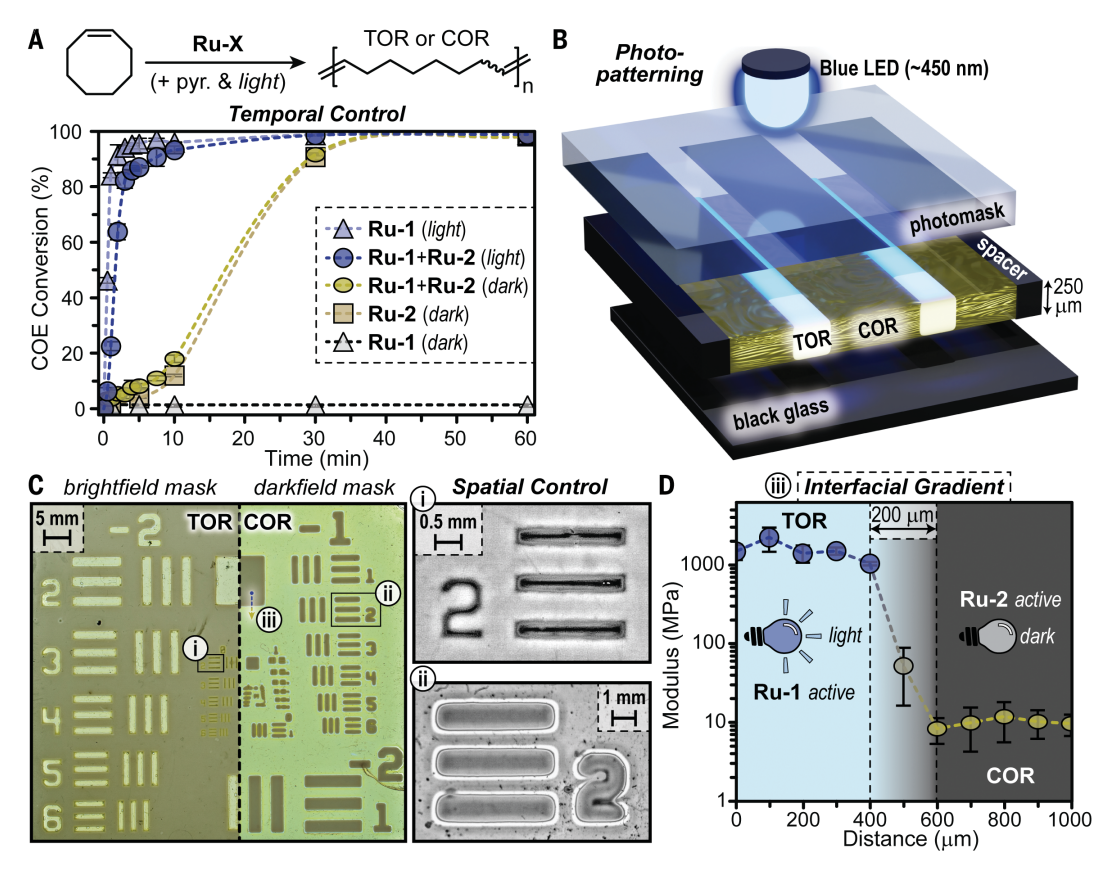
visible light. Of the three derivatives, only Ru-1 was inactive in the absence of light (<1% conversion of COE, 50 ppm catalyst, 75 ppm pyr., ~23°C, 1 hour), which is attributed to the steric hindrance and Lewis basicity of indenylidene (18). Irradiation with a blue LED resulted in quantitative COE consumption, indicating excellent temporal control (~460 nm, 170 mW/cm², ~23°C, 5 min) (Fig. 1C and table SI). The resulting TOR polymers had a *trans* content of 91%, a modest increase relative to those obtained through thermal activation (78% *trans*), possibly arising from a decrease in polymerization temperature.

Polyoctenamers with high *cis*-alkene content, *cis* polyoctenamer rubber (COR), were achieved

by examining four commercial stereoregulating catalysts (Fig. 1B and fig. S11) (*16*, *19*). The stereoselective catalysts (i.e., double-bond configuration defined by the catalyst) were unable to reach high conversions of COE at both room and elevated temperatures (<30%, 100°C, 18 hours). Conversely, low concentrations (20 ppm relative to COE) of the stereoretentive catalysts (i.e., double-bond configuration defined by the monomer) proved effective at reaching high conversions of COE (>99%, ~23°C, <2 hours) to produce COR with a *cis* content of ~99% (Fig. 1C and table S1).

The mechanical properties of TOR and COR were examined under uniaxial tension until failure (Fig. 2A, table S5, and figs. S24 to S27).

Fig. 3. Spatiotemporal control over polyoctenamer stereochemistry. (A) Polymerization kinetics of COE with various catalyst systems, pyr. is present in all examples containing Ru-1. Data points represent an average of three independent polymerizations with error bars of ±1 SD from the mean. (B) Illustration of photopatterning setup. (C) Images of photopatterned TOR and COR prepared using 1951 USAF bright-field and dark-field photomasks. Leftmost patterns are two backlit images of separate films digitally stitched together to show the effect of inverting the majority phase from TOR (left of dashed line) to COR (right of dashed line). Regions (i) and (ii) were examined with a backlit digital microscope, providing the magnified images shown to the right. The arrow labeled (iii) represents the position and direction of nanoindentation testing, providing modulus as a function of position across the TOR/COR interface (D). Data points represent an average of six indentations with error bars of ±1 SD from the mean.



Five different polymerization conditions were analyzed: (i) G2 (50 ppm) with trimethyl phosphite (50 ppm) (20) to facilitate thermally latent casting (80°C, 1 hour); (ii) Ru-1 (50 ppm) and pyr. (75 ppm) with blue light irradiation  $(\sim 460 \text{ nm}, \sim 170 \text{ mW/cm}^2, 5 \text{ min}); (iii) \text{ Ru-}2$ (20 ppm, room temperature, 1 hour); and (iv and v) Ru-1 (50 ppm), pyr. (75 ppm), and Ru-2 (20 ppm) with (5 min) (iv) or without (60 min) (v) light irradiation. Conditions that produced TOR (conditions i, ii, and iv) gave strong, stiff materials with a maximum stress ( $\sigma_m$ ) from ~23 to 27 MPa and a Young's modulus (E) from ~800 to 1000 MPa. By contrast, conditions that produced COR (conditions iii and v) provided a soft and stretchable material, with  $\sigma_{\rm m} \approx 12$  MPa,  $E \approx 3$  MPa, and strain at failure ( $\varepsilon_f$ ) of ~800%. This mechanical behavior resembles that of conventional thermoplastic elastomers such as self-assembled polyolefin block copolymers (21, 22); however, the composition and architecture of COR are those of a simple rubbery homopolymer. Specifically, at small strains, ( $\lesssim 100\%$ ) the hysteresis of COR was low and comparable to that of natural rubber (fig. S25), whereas at large strains, COR yields and plastically deforms ( $\varepsilon$ >100%; Fig. 2A), similar to other thermoplastics such as styrene-isoprene-styrene of low styrene fraction. Therefore, the mechanical properties of polyoctenamer could be substantially varied with mixtures of Ru-1 and Ru-2 catalysts by simply toggling visible light-emitting diode (LED) irradiation.

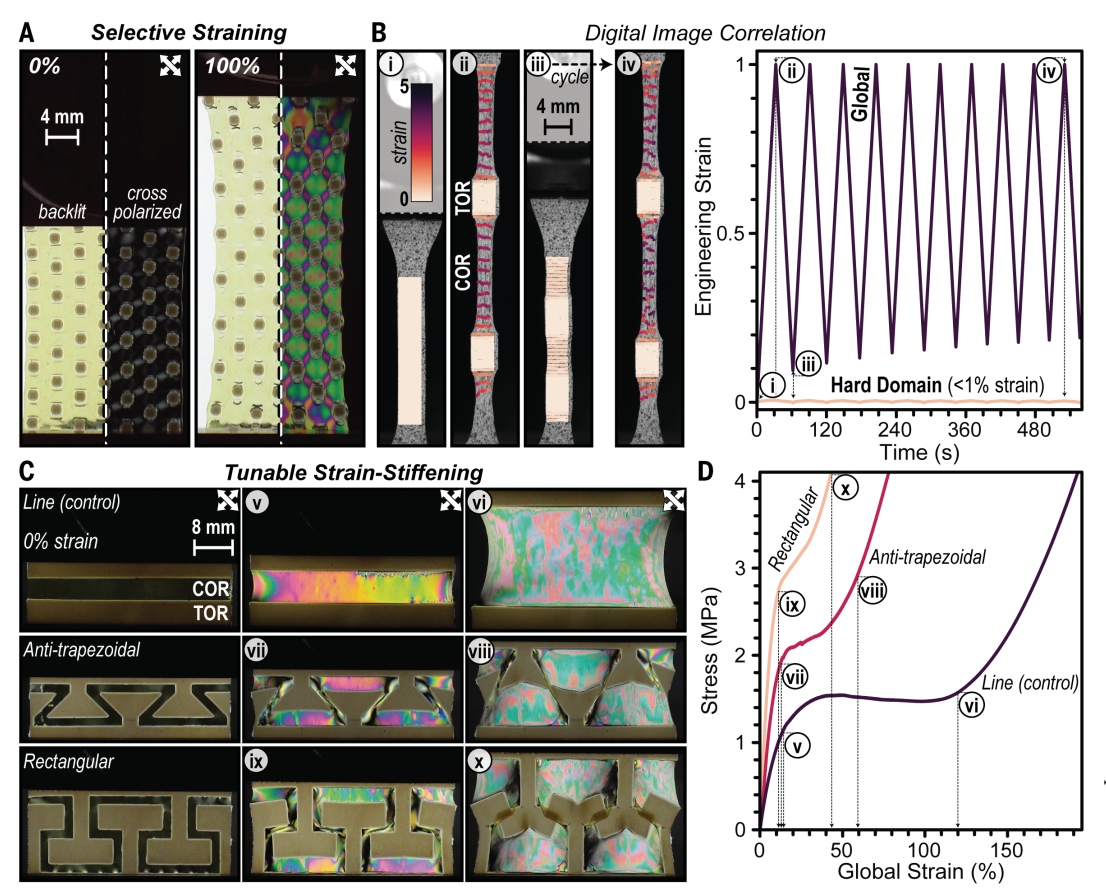
This difference in mechanical properties was hypothesized to stem from backbone stereochemistry and crystallization. TOR is opaque with visible light transmittance <1%, whereas COR is transparent (fig. S28), indicating that high trans content leads to more crystalline polymer domains. Differential scanning calorimetry was used to characterize the melting temperature  $(T_m)$  and degree of crystallinity (Fig. 2B and figs. S29 and S30). Using a modulated heat ramp and integrating the change in enthalpy versus "100%" crystalline polyoctenamer (216 J/g) (23) provided a  $T_{\rm m} \approx$ 72°C and ~65% crystallinity for TOR and a  $T_{\rm m} \approx 16^{\circ}{\rm C}$  and ~20% crystallinity for COR. In addition, a  $T_{\rm sc} \approx -80^{\rm o}$ C was identified for both TOR and COR (fig. S31), confirming that at room temperature. TOR is a semicrystalline thermoplastic with mechanical properties strongly influenced by the crystalline domains, and COR is an amorphous polymer melt.

The observation that COR was fracture resistant prompted the characterization of its fracture energy (i.e., toughness) as measured by the critical energy release rate ( $G_c$ ). Precracked, pure-shear specimens of polyocten-

amers were uniaxially stretched until failure, and  $G_{\rm c}$  was calculated as  $W_{\rm PS} \times h_0$  (24), where  $W_{\rm PS}$  is the strain energy density in the bulk at the critical stretch of crack propagation and  $h_0$  is the initial specimen height (Fig. 2C, fig. S32, and table S6). This analysis revealed  $G_c$ values of 150  $\pm$  40 kJ/m<sup>2</sup> (Ru-2, dark) and  $190 \pm 40 \text{ kJ/m}^2$  (Ru-1+Ru-2, dark) for COR and  $10 \pm 3 \text{ kJ/m}^2$  (Ru-1+Ru-2, light) for TOR (Fig. 2D). Compared with commercial materials, COR was an order of magnitude tougher than soft elastomers (E < 10 MPa), such as rubbers and polyurethanes 40A and 90A, and equivalent to the polyurethane Elastollan ( $G_c = 138 \pm$  $13 \text{ kJ/m}^2$  and E = 7 MPa) (25). Conversely, TOR had a toughness between that of other stiff plastics such as acrylonitrile butadiene styrene (ABS) and high-density polyethylene (HDPE) (Fig. 2D, fig. S32, and table S6). Furthermore, lowering the Ru-2 catalyst concentration from 20 to 3.3 ppm increased the  $G_c$  to 280  $\pm$  17 kJ/m<sup>2</sup> (figs, S33 to S35), which is postulated to arise from the increased COR molecular weight (figs. S36 to S38). Thus, stereoregulated ROMP of COE provides a facile pathway to designing soft and tough materials for applications that require large deformations at "soft/hard" interfaces, such as wearable electronics (26).

The role of crystallinity on the mechanical properties of polyoctenamers was further

Fig. 4. Mechanical metamaterial characterization. (A) Images of backlit array of TOR squares in a COR matrix with and without crossed polarizers at 0 and 100% strain. (B) Images of a patterned sample during the first and last strain cycles used for digital image correlation analysis. (C and D) Images of backlit samples between crossed polarizers during uniaxial tension applied vertically, showing the effect of suture design on strain-stiffening behavior (C) and corresponding stressstrain curves (D).



assessed and compared with natural rubber using a combination of birefringence (Fig. 2E and fig. S39) and wide-angle x-ray scattering (WAXS) (Fig. 2F and figs. S40 to S44). At low strains (100%), both natural rubber and COR showed a stress concentration in the vicinity of the crack tip, whereas at larger strains (500%), COR distinctly delocalized the stress and dissipated energy by undergoing plastic deformation throughout the bulk (movies S1 and S2). Characterization with WAXS confirmed that at room temperature, COR was amorphous before stretching but crystallized when deformed above 100% (Fig. 2F). Thus, like natural rubber, COR is first toughened by strain-induced crystallization but then dissipates elastic energy both in the vicinity of the crack tip and in the bulk to erase the stress concentration that constitutes a driving force for fracture.

The ability to control the stereochemistry and mechanical properties of polyoctenamers enabled photopatterning TOR and COR from COE using a mixed-catalyst system with Ru-1 (50 ppm + 75 ppm pyr.) and Ru-2 (20 ppm). ROMP kinetics for different catalyst systems were characterized by <sup>1</sup>H NMR spectroscopy (Fig. 3A and figs. S20 to S23). Blue light irradiation (~460 nm, ~170 mW/cm²) of the mixed-catalyst system in COE resulted in ~90% conversion to TOR in ~5 min, comparable to

the control without Ru-2. By contrast, the mixedcatalyst system in the dark resulted in relatively slow COR formation: <10% conversion in ~5 min. However, after ~60 min in the dark. COE was fully consumed, forming COR, and this was comparable to what happened in the control without Ru-1 and pyr. present. This method also enabled fabrication of thick TOR specimens with trans-alkene contents of ~80% up to a depth of ~4 mm (fig. S45), likely due to the low concentration and photobleaching of pyr. (75 ppm) during photoinduced ROMP. These distinct differences in light versus dark ROMP kinetics enabled photopatterning of stiff TOR domains in a soft COR matrix.

To pattern TOR domains in a COR matrix, the mixed-catalyst system in COE was loaded between a photomask and black glass separated by 250- $\mu$ m shims and irradiated with blue light for 5 min (Fig. 3B and figs. S46 and S47). Pattern fidelity was characterized using both bright-field and dark-field 1951 USAF standardized photomasks, which define resolution as the smallest discernible line pair (Fig. 3C). The resolution for bright-field (majority TOR) and dark-field (majority COR) was ~9.0 line pairs/mm (~55  $\mu$ m) and ~1.3 line pairs/mm (~400  $\mu$ m), respectively, with differences hypothesized to arise from crystal growth outside of irradiated areas, as evidenced by features

smaller (Fig. 3Ci) and larger (Fig. 3Cii) than those on the mask. Nanoindentation at a TOR/COR interface (Fig. 3Ciii) also revealed a change in  $\it E$  from ~1000 to ~10 MPa over ~200  $\mu m$ , consistent with differences in polyoctenamer stereochemistry and crystallinity and the mechanical properties of TOR and COR (Fig. 3D and fig. S48).

As a final proof of concept, patterns were designed to access unusual bulk mechanical behaviors (i.e., metamaterials) that require synergy between stiff and soft domains (Fig. 4). First, selective straining was demonstrated with a square array of TOR patterned into a continuous COR matrix, a construct with potential utility as a substrate for stretchable electronics (27). Cycling these specimens to 100% strain qualitatively showed that deformation was localized in the soft COR domains (Fig. 4A and movie S3). Quantification of this behavior using digital image correlation on a specimen containing 5-mm-wide lines revealed <1% strain in the TOR domains relative to the bulk (Fig. 4B, figs. S49 to S51, and movie S4). Thus, TOR may act as a support structure (i.e., substrate) for brittle (electronic) components in stretchable devices. Moreover, the mitigation of interfacial failure upon application of substantial global stress (>4 MPa) suggests the presence of strongly interwoven domains, which may result from a combination of tie chains and physical entanglements between TOR and COR and/or continuity of TOR/COR polymer backbones as a result of crossmetathesis.

More sophisticated sutures were also examined as a means to control strain stiffening, a common mechanism used by natural tissue to prevent rupture (28) (Fig. 4C). Three patterns holding constant COR:TOR ratios (~0.35:0.65) were characterized by uniaxial tension between crossed polarizers. Straight-line (control), antitrapezoidal, and rectangular sutures showed stress-strain localization on COR. Distinct strainstiffening behavior was apparent for each suture pattern due to the increase in stress that occurs as regions of TOR approach each other at specific global strain values (Fig. 4D, fig. S52, and movies S5 to S7). Thus, photopatterning of polyoctenamer stereochemistry enables the bulk preparation of mechanical metamaterials.

This report describes a simple and scalable synthetic method to prepare polymeric multimaterials with stiff (TOR) and elastic (COR) domains. Specifically, a mixed-catalyst system sensitive to visible light enables ROMP of COE with spatiotemporal control over the resultant polyoctenamer backbone stereochemistry. Polyolefins with a combination of toughness, elasticity, and moduli were patterned with microscopic precision, providing access to materials with mechanically robust "hard/soft" interfaces.

#### REFERENCES AND NOTES

1. W. Huang et al., Adv. Mater. 31, e1901561 (2019).

- F. Barthelat, Z. Yin, M. J. Buehler, *Nat. Rev. Mater.* 1, 16007 (2016).
- N. Reznikov, M. Bilton, L. Lari, M. M. Stevens, R. Kröger, Science 360, eaao2189 (2018).
- M. S. Ganewatta, Z. Wang, C. Tang, Nat. Rev. Chem. 5, 753–772 (2021).
- 5. Y. Fang et al., Chem. Rev. 122, 5233-5276 (2022).
- 6. X. Zhao et al., Chem. Rev. 121, 4309-4372 (2021).
- M. Li, A. Pal, A. Aghakhani, A. Pena-Francesch, M. Sitti, Nat. Rev. Mater. 7, 235–249 (2022).
- T. Someya, Z. Bao, G. G. Malliaras, *Nature* **540**, 379–385 (2016).
- 9. L. M. Cox et al., Adv. Eng. Mater. 21, 1900578 (2019).
- 10. S. Bialas et al., Adv. Mater. 31, e1807288 (2019).
- 11. N. D. Dolinski et al., Adv. Mater. 30, e1800364 (2018).
- 12. J. J. Schwartz, A. J. Boydston, *Nat. Commun.* **10**, 791 (2019). 13. Y. Ma *et al.*, *J. Am. Chem. Soc.* **143**, 21200–21205 (2021).
- Z. Wang et al., Proc. Natl. Acad. Sci. U.S.A. 116, 5967–5972 (2019).
- O. Eivgi, R. S. Phatake, N. B. Nechmad, N. G. Lemcoff, Acc. Chem. Res. 53, 2456–2471 (2020).
- 16. J. A. Song et al., J. Am. Chem. Soc. 142, 10438–10445 (2020).
- C. Theunissen, M. A. Ashley, T. Rovis, J. Am. Chem. Soc. 141, 6791–6796 (2019).
- F. Boeda, H. Clavier, S. P. Nolan, Chem. Commun. 24, 2726–2740 (2008).
- K. Endo, R. H. Grubbs, J. Am. Chem. Soc. 133, 8525–8527 (2011).
- 20. I. D. Robertson et al., ACS Macro Lett. 6, 609-612 (2017).
- A. Hotta et al., Proc. Natl. Acad. Sci. U.S.A. 103, 15327–15332 (2006).
- C. Creton, G. Hu, F. Deplace, L. Morgret, K. R. Shull, Macromolecules 42, 7605–7615 (2009).
- 23. W. A. Schneider, M. F. Müller, J. Mol. Catal. 46, 395-403 (1988).
- 24. R. S. Rivlin, A. G. Thomas, J. Polym. Sci. 10, 291-318 (1953).
- 25. G. Scetta, N. Selles, P. Heuillet, M. Ciccotti, C. Creton, Polym. Test. 97, 107140 (2021).
- S. Wang, J. Y. Oh, J. Xu, H. Tran, Z. Bao, Acc. Chem. Res. 51, 1033–1045 (2018).
- 27. R. Libanori et al., Nat. Commun. 3, 1265 (2012).
- 28. Z. Liu, Z. Zhang, R. O. Ritchie, *Adv. Funct. Mater.* **30**, 1908121 (2020).

#### **ACKNOWLEDGMENTS**

We thank Umicore for supplying ruthenium catalysts M320, M800 (Ru-1), M2001, and M2002 and C. Tagnon for assistance with the

preparation of Fig. 3B. Funding: This work was supported primarily by the National Science Foundation (grant no. DMR-2045336 to A.K.R., H.L.C., K.S.M., and Z.A.P. and a graduate research fellowship under grant no. DGE-1610403 to M.J.A.; film fabrication, catalyst system development, characterization, and supervision). This work was supported in part by the U.S. Department of Energy, Office of Science, Basic Energy Sciences, Energy Frontier Research Center, Center for Materials for Water and Energy Systems (M-WET) (grant no. DE-SC0019272 to M.J.A. and B.D.F.; supervision); the Robert A. Welch Foundation (grant no. F-2007 to Z.A.P.; materials and supplies); the American Chemical Society Petroleum Research Fund (grant no. 60802-DNI7 to Z.A.P.; materials and supplies); and the UT Cockrell School of Engineering (A.J.A. and G.E.S.; mechanical testing). The authors acknowledge use of the UT NMR facilities (NIH grant no. 1 S10 OD021508-01). Author contributions: Conceptualization (A.K.R., M.J.A., Z.A.P.); Funding acquisition (B.D.F., G.E.S., Z.A.P.); Investigation (A.K.R., H.L.C., K.S.M., M.J.A., A.J.A.); Methodology (A.K.R., H.L.C., K.S.M., M.J.A., A.J.A., G.E.S., Z.A.P.); Project administration (Z.A.P.); Supervision (B.D.F., G.E.S., Z.A.P.); Visualization (A.K.R., H.L.C., K.S.M., M.J.A., A.J.A., Z.A.P.); Writing original draft (A.K.R., Z.A.P.); Writing - review and editing (A.K.R., H.L.C., K.S.M., M.J.A., A.J.A., B.D.F., G.E.S., Z.A.P.). Competing interests: US provisional patent application no. 63/351,868 ("Cyclic olefin polymer having high Cis double bond content") was filed 14 June 2022 by Z.A.P. and A.K.R. The remaining authors declare no competing interests. Data and materials availability: All data are available in the main text or the supplementary materials. License information: Copyright © 2022 the authors, some rights reserved; exclusive licensee American Association for the Advancement of Science. No claim to original US government works. https://www. science.org/about/science-licenses-journal-article-reuse

#### SUPPLEMENTARY MATERIALS

science.org/doi/10.1126/science.add6975
Materials and Methods
Supplementary Text
Figs. S1 to S55
Tables S1 to S6
References (29–38)
Movies S1 to S8
AutoCAD Data S1

Submitted 28 June 2022; accepted 21 September 2022 10.1126/science.add6975



## Polymeric multimaterials by photochemical patterning of crystallinity

Adrian K. RylskiHenry L. CaterKeldy S. MasonMarshall J. AllenAnthony J. ArrowoodBenny D. FreemanGabriel E. SanojaZachariah A. Page

Science, 378 (6616), • DOI: 10.1126/science.add6975

#### A reactive way to make a composite

Blending different materials to form a composite is a way to tune properties to achieve something not possible in a single material. However, it can be challenging to mix or pattern dissimilar materials. Rylski *et al.* developed a way to produce multimaterials by patterning a strong domain within an elastic domain. They used a dual-catalyst system that polymerizes *cis*-polycyclooctene in the dark but forms *trans*-polycyclooctene when exposed to light. This approach led to a polyoctenamer with cohesively connected viscoelastic (soft) and semicrystalline (hard) domains and provided the ability to spatially control the properties of the polymer. —MSL

### View the article online

https://www.science.org/doi/10.1126/science.add6975

#### **Permissions**

https://www.science.org/help/reprints-and-permissions

Use of this article is subject to the Terms of service